CHAPTER TWENTY

A SHALLOW WATER DIRECTIONAL WAVE RECORDER

S.J. Buchan, R.K. Steedman, S.A. Stroud, D.G. Provis

ABSTRACT

Shallow water wave theory shows that estimates of directional wave climate may be obtained from the measurement of near-bottom pressure and horizontal velocity components. Recent developments in low powered sensors and high density data loggers, incorporated into a bottom-mounted directional wave recorder, make the collection of directional shallow water wave data possible on a routine basis. The instrument is compact, robust, reliable and easily manageable from small craft, providing deployment capacities of up to four months. Analysis methods have been developed which provide for conversion of the recorded data to useful, convenient information.

1.   INTRODUCTION

During recent years, recognition of the importance of directional wave information in many facets of coastal and ocean engineering design has been increasing. Goda et al. (1978) have illustrated the importance of wave directionality for studies of wave diffraction and refraction in harbours; Forristall et al. (1978) have demonstrated the inadequacies of uni-directional wave theories in describing wave kinematics; and Sand et al. (1981) have discussed the applications of directional wave information to the hydrodynamics and design of offshore structures and pipelines.

Advances in remote low powered logger and sensor technology have allowed the development of reliable, compact, robust and manageable water current and pressure measuring devices. In May 1980, Sea Data Corporation were commissioned to modify their 635-11 Wave and Tide Recorder (based on bottom-mounted pressure measurements) to include synchronous horizontal velocity measurements within each "burst" of pressure data. The result was the Sea Data 635-12S Directional Wave and Tide Recorder, the use of which is the subject of this paper. Reference is made to the instrument operation and to the underlying theory on which the data analyses are based. Various analysis techniques are illustrated, and verification of instrument and analysis performance is provided.

---

*   R.K. Steedman & Associates
     384 Rokeby Road, Subiaco 6008, Western Australia

2.   INSTRUMENTATION

The instrument measures fluctuations in absolute pressure and
horizontal current velocity, at both tide and wind wave frequencies.
Instrument temperature is also logged. A complete description of the
instrument is given by Aubrey and Hill (1984), and a detailed analysis
of sensor specifications is given by Grosskopf et al. (1983).

In operation the 635-12S runs two separate sampling schemes in
parallel. These are the mean (tide) and burst (wave) recording modes.
Data from each mode are recorded in an interleaved format on a
magnetic cassette tape.

In the mean mode, water pressure is integrated continuously over a
specified sample interval. To conserve battery power, the mean
current is computed only over every eighth mean pressure sample
interval. The mean sample interval may be selected in the range 3.75
to 60 minutes. An instantaneous temperature measurement from a
thermistor within the instrument housing is sampled after every 8 mean
pressure samples. Data recording takes place every 8 sample intervals
when an elapsed time, 8 tide measurements, a water temperature
measurement and the mean current components are recorded.

In burst mode, the instrument rapidly samples the water pressure and
the two current velocity components at a preset interval in the range
0.5 to 4 seconds. The number of samples in each burst may be adjusted
in steps between 64 and 2048, or alternatively the instrument may be
set to run continuously. The interval between bursts may be varied
from 0.5 to 24 hours. The burst samples are recorded as triples of
the water pressure, easterly and northerly current components.

3.   DEPLOYMENT AND RETRIEVAL

The directional wave recorder is usually deployed in an aluminium
tripod which is lowered to the sea bed by winch from a work vessel.
The tripod is attached to small surface floats by a buoyant line, to
facilitate recovery. Thus, deployment and retrieval operations can be
carried out without diver assistance.

Within the tripod, the velocity and pressure sensors are located at
1.5 m above the base. Provided the sea bed is relatively smooth and
flat (easily checked using an echo sounder), then the sensors should
be located above the bottom boundary layer.

An alternative deployment arrangement is provided by fixing the
directional wave recorder to an offshore pile. This arrangement
allows the sensors to be located near the water surface, but can only
be used when the pile wake effects are not of significance.
Deployment and retrieval of the instrument using this arrangement does
require diver assistance.

4.   UNDERLYING THEORY

To obtain a representation of the surface sea state from subsurface
measurements of pressure and velocity, an appropriate theory
describing the kinematics of flow beneath surface waves must be
applied. An assessment of available wave theories is presented in
Forristall et al. (1978).

The simplest approach is to use linear wave theory which may be
extended through spectral concepts to model irregular (i.e. aperiodic)
sea. The most serious deficiency of linear theory occurs due to the
non-linearity of the free surface boundary condition.

Higher order regular (periodic) and irregular (aperiodic) theories
provide a better match to the free surface boundary condition, but
their complexity precludes their incorporation in any practical
analysis of directionally spread sea states.

From analysis of measurements conducted during Tropical Storm Delia in
the Gulf of Mexico, Forristall et al. (1978) demonstrated that using a
linear theory which accounted for the directional nature of the
measured sea state provided a better representation of wave kinematics
than higher-order, uni-directional wave theories.

Linear Wave Theory :   A linear representation of the surface
elevation η, above or below the equilibrium water level, of an
abritrary cosine wave component of a random sea is given by,

$$\eta = \alpha \cos(kx \cos\theta + ky \sin\theta - 2\pi ft + \phi) \tag{1}$$

This formulation has been set in a right-hand, rectangular coordinate
system (x,y,z) with z chosen as positive upward from the sea bed where

   α is the wave amplitude;

   θ is the direction of phase propagation, measured
      counter-clockwise from the x axis;

   ϕ is the wave phase;

   t is time;

   k is the horizontal wave number;

   f is the wave frequency in cycles per second.

The horizontal wave number $k = 2\pi/\lambda$, where λ is the wave length.

A freely propagating surface gravity wave described by the above
formula should satisfy a dispersion relation given by,

$$(2\pi f)^2 = gk \tanh kd \tag{2}$$

where g is the acceleration due to gravity, and d is the water depth.

At any level z in the water column below such a wave, the horizontal velocity components are described by,

$$u = \alpha 2\pi f \, \frac{\cosh kz}{\sinh kd} \, \cos\theta \, \cos(kx \cos\theta + ky \sin\theta - 2\pi ft + \phi) \quad , \quad (3)$$

and

$$v = \alpha 2\pi f \, \frac{\cosh kz}{\sinh kd} \, \sin\theta \, \cos(kx \cos\theta + ky \sin\theta - 2\pi ft + \phi) \quad . \quad (4)$$

the wave-induced pressure at z is given by,

$$p = \alpha \rho g \, \frac{\cosh kz}{\cosh kd} \, \cos(kx \cos\theta + ky \sin\theta - 2\pi ft + \phi) \qquad , \qquad (5)$$

where ρ is the water density.

A confused sea state may be represented by a summation of linear waves, given by (1), at various frequencies, propagation directions and phases, and may be described by a "random" sum

$$\eta(x,y,t) = \sum_m \sum_n \alpha_{mn} \cos\psi_{mn} \qquad , \qquad (6)$$

where the indices m,n run over selected frequencies and directions respectively, and the composite phase function is given by

$$\psi_{mn} = \psi_{mn}(x,y,t)$$
$$= k_m x \cos\theta_n + k_m y \sin\theta_n - 2\pi f_m t + \phi_{mn} \qquad . \qquad (7)$$

In the above, ϕ_{mn} is the random phase for the (m,n) wavelet, assumed to be uniformly distributed over the direction interval $(0, 2\pi)$ and independent from wavelet to wavelet.

According to linear theory, the kinematics of a confused sea state described by (6) may be obtained by superposition from equations (3) to (5) as:

$$u(x,y,z,t) = \sum_m \sum_n \alpha_{mn} \, 2\pi f_m \, \frac{\cosh k_m z}{\sinh k_m d} \, \cos\theta_n \, \cos\psi_{mn} \qquad , \qquad (8)$$

$$v(x,y,z,t) = \sum_m \sum_n \alpha_{mn} \, 2\pi f \, \frac{\cosh k_m z}{\sinh k_m d} \, \sin\theta_n \, \cos\phi_{mn} \qquad , \qquad (9)$$

and

$$p(x,y,z,t) = \sum_m \sum_n \alpha_{mn} \, \rho g \, \frac{\cosh k_m z}{\cosh k_m d} \, \cos\psi_{mn} \qquad , \qquad (10)$$

where $u(x,y,z,t)$ is the x component of the water particle velocity at space location (x,y,z) at some time t. Similarly, $v(x,y,z,t)$ is the y component velocity and $p(x,y,z,t)$ is the pressure.

Spectral Representation of Wave Properties :   In practice, p,u,v
measurements are taken over time at the same horizontal location, i.e.
setting $(x,y) = (0,0)$. Further, (u,v) measurements are made at the
same height $z = z_v$ above the sea bed. Pressure measurements may be
made at a different height $z = z_p$. It is important that z_p and z_v are
chosen to be above the bottom boundary layer.

We may introduce a frequency domain description of the wave field.
The spectral density, $S(f_m, \theta_n)$, of the surface elevation is related
to the mean (or expectation) of the square of the random amplitude,
$E(\alpha_{mn}^2)$, by

$$S(f_m, \theta_n) = \frac{1}{2\Delta f_m \Delta \theta_n} E(\alpha_{mn}^2) \qquad , \quad (11)$$

where Δf_m and $\Delta \theta_n$ are the increments of frequency and direction
"occupied" by the (m,n) wave component.

By taking lagged products of measured quantities (p,u,v) and passing
from summation to integration, cross-covariances of p,u and v may be
formed (Borgman, 1979). Fourier transformation of the cross-
covariances provides the following cospectral expressions which may be
used to estimate the direction surface sea state:

$$c_{uu}(f) = A^2(f) \int_o^{2\pi} S(f,\theta) \cos^2\theta \, d\theta \qquad , \quad (12)$$

$$c_{uv}(f) = A^2(f) \int_o^{2\pi} S(f,\theta) \sin\theta \cos\theta \, d\theta \qquad , \quad (13)$$

$$c_{vv}(f) = A^2(f) \int_o^{2\pi} S(f,\theta) \sin^2\theta \, d\theta \qquad , \quad (14)$$

$$c_{pp}(f) = B^2(f) \int_o^{2\pi} S(f,\theta) \, d\theta \qquad , \quad (15)$$

$$c_{up}(f) = A(f)B(f) \int_o^{2\pi} S(f,\theta) \cos\theta \, d\theta \qquad , \quad (16)$$

$$c_{vp}(f) = A(f)B(f) \int_o^{2\pi} S(f,\theta) \sin\theta \, d\theta \qquad , \quad (17)$$

where

$$A(f) = 2\pi f \frac{\cosh kz_v}{\sinh kd} \qquad , \quad (18)$$

and

$$B(f) = \rho g \; \frac{\cosh kz_p}{\cosh kd} \qquad , \quad (19)$$

represent velocity and pressure attenuation functions, respectively.

The Directional Spreading Function :   Progress in the determination of the spectral density function $S(f,\theta)$ is made by recasting the function as

$$S(f,\theta) = E(f) \; H(f,\theta) \qquad , \quad (20)$$

with the constraint

$$\int_o^{2\pi} H(f,\theta) \; d\theta = 1 \qquad . \quad (21)$$

In the above, the directional energy spectrum $S(f,\theta)$ has been separated into a non-directional energy spectrum $E(f)$, and a directional spreading function $H(f,\theta)$. $E(f)$ represents the surface wave energy summed over all propagation directions, i.e.

$$E(f) = \int_o^{2\pi} S(f,\theta) \; d\theta \qquad . \quad (22)$$

$H(f,\theta)$ describes the distribution of the total energy $E(f)$ over all possible propagation directions θ. Its estimation is the key to obtaining a directional description of a sea state.

Following Longuet-Higgins et al. (1963), a convenient approximation to the directional spreading function may be obtained by expansion of $H(f,\theta)$ in a truncated Fourier series, such that

$$H(f,\theta) = \frac{1}{2\pi} + \sum_{m=1}^{M} (a_m \cos m\theta + b_m \sin m\theta) \qquad . \quad (23)$$

The p, u, v measurements which form the basis of this directional wave analysis contain sufficient information for the estimation of the above Fourier series truncated at $M = 2$.

Parametric Description of the Directional Spreading Function :
Further improvement to the description of the directional sea state may be obtained by introducing a subjectively selected, parametric approximation to the directional spreading function, $H(f,\theta)$. A model which has been widely used is that of Longuet-Higgins et al. (1963),

$$
\begin{aligned}
H(f,\theta) &= \frac{\Gamma(s+1)}{2\sqrt{\pi} \; \Gamma(s+1/2)} \; \cos^{2s}\left[(\theta-\theta_o)/2\right] \\[2mm]
&= (1/\pi) \left[1/2 + \sum_{n=1}^{\infty} (r_n \cos n\theta_o) \cos n\theta \right. \\[2mm]
&\qquad\qquad\qquad\qquad\qquad\qquad\qquad\qquad\qquad , \quad (24) \\[2mm]
&\qquad\qquad \left. + \sum_{n=1}^{\infty} (r_n \sin n\theta_o) \sin n\theta \right]
\end{aligned}
$$

where

$$r_n = \frac{\Gamma^2(s+1)}{\Gamma(s+n-1) \ \Gamma(s-n+1)}$$

In the above, s is referred to as the "sharpness index", and θ_o is the predominant direction of wave propagation. The multiplying term involving the Gamma function Γ arises from the constraint equation (13). This model should provide a satisfactory description of a unimodal wave field with wave directions dispersed over a narrow sector centred about θ_o. A high value of "sharpness index" indicates that all wave directions are concentrated about θ_o.

5.   ANALYSIS TECHNIQUES

<u>Primary Data Plots</u> :   The wave-induced velocity data returned from each "burst" of the Sea Data 635-12S are illustrated by the cross plots of the horizontal current velocity components (figure 1).
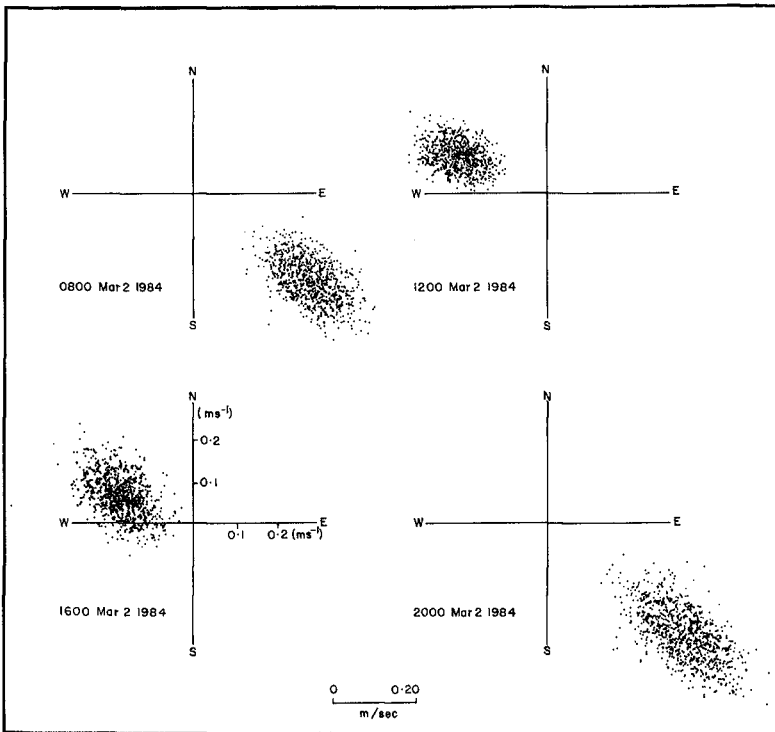

Figure 1   Example cross plots of the u-v horizontal current velocities measured near the sea bed. The elliptical scatter is caused by wave-induced currents, and displaced by tidal currents.

The velocity cross plot shows the elliptical spread of horizontal
wave-induced motions. The principle direction of wave propagation is
along the major axis of the ellipse. The 180° ambiguity about the
direction of phase propagation is resolved by examination of the
pressure time history. Horizontal wave-induced velocities under wave
crests are in the same direction as the phase propagation.

Frequency Domain Estimation of Directional Parameters :   The
directional spectrum of a random sea state may be estimated from
Fourier transformations of a set of N triplets of simultaneous u,v,p
measurements, consecutively sampled at a time spacing of Δt.

Fourier transformations of the measured p,u,v time series provide
estimates of the left-hand sides of equations (12) to (17), the p,u,v
cospectra. Using the velocity and pressure attenuation functions (18)
and (19) determined from linear wave theory, and the description of
the spectral density function given by (20) to (22), the coefficients
a_1, b_1, a_2 and b_2 of the truncated Fourier expansion of the spreading
function (23), may be estimated from the p,u,v cospectra.

First order estimates of the directional spectral parameters of the
$\cos^{2s} [(\theta - \theta_o)/2]$ model may be obtained by comparing equation (24) with
equation (23), from which

$$s = \frac{r_1}{1 - r_1} \qquad (25)$$

where

$$r_1^2 = a_1^2 + b_1^2 \qquad , \quad (26)$$

and

$$\theta_o = \arctan \left(\frac{b_1}{a_1} \right) \qquad , \quad (27)$$

which are obtained from the pressure-velocity cospectra.

An alternative estimate of s and θ_o, known as the second order fit, is
also available, as

$$s = \frac{(1 + 3r_2) + (1 - 14r_2 + r_2^2)^{1/2}}{2(1 - r_2)} \qquad (28)$$

where

$$r_2^2 = a_2^2 + b_2^2 \qquad , \quad (29)$$

and

$$\theta_o = \frac{1}{2} \arctan \left(\frac{b_2}{a_2} \right) \qquad . \quad (30)$$

which is obtained from velocity-velocity cospectra.

An example of the directional spectral information attainable from
each "burst" of p,u,v measurements of the Sea Data 635-12S Directional
Wave and Tide Recorder is presented in figure 2. First and second
order estimates of wave direction agree very well. First and second
order estimates of sharpness index are not theoretically equivalent,
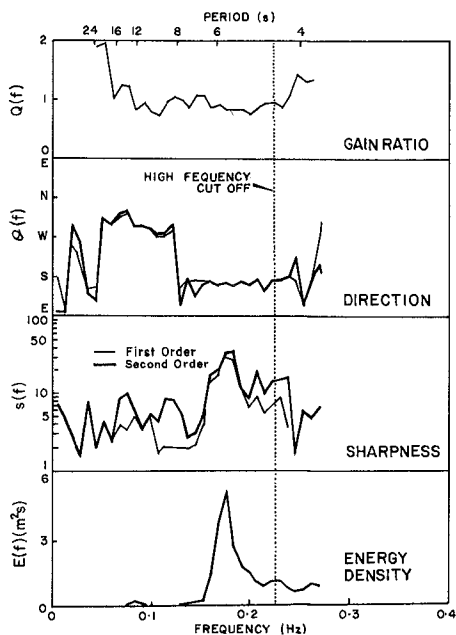but are expected to display similar trends.

Figure 2   Example of the spectral information attainable from each
           "burst" of a directional wave recorder. First and second
           order estimates are derived from equations (25) to (27) and
           (28) to (30), respectively.

Following the example of Forristall et al. (1978) the gain ratio Q(f)
has also been calculated. It represents the ratio of the measured
pressure to velocity transfer function and that predicted by linear
theory. From equations (18) and (19), $Q(f) = A(f)/B(f)$. If $Q(f)$
remains near unity, linear theory is providing a satisfactory
description of wave kinematics. Figure 2 shows that $Q(f)$ departs from
unity for very high frequencies where ambient turbulence contaminates
the data, and for low frequencies where surface wave energy is very
low.

Also presented on this plot is a dotted vertical line which marks
where the spectral moment computations have been truncated (high
frequency cut off), to avoid the increasing noise contamination of the
wave signal.

Time Domain Estimation of Directional Parameters :   The mean wave
direction and sharpness index estimates may be obtained without
recourse to spectral analysis, from the covariance (time domain)
equivalents of equations (25), (27), (28) and (30). For each set of N
triplets of p,u,v the variances and covariances $C_{\gamma\zeta}$ of the measured
quantities are computed by taking the dot products as follows:

$$C_{\gamma\zeta} = \frac{1}{N} \sum_{i=1}^{N} (\gamma_i - \bar{\gamma})(\zeta_i - \bar{\zeta}) \qquad ,$$

where the overbars denote sample means, and the subscripts γ and ζ
denote p, u or v.

First order estimates of mean direction $\bar{\theta}$ and sharpness index $\bar{s}$ are
obtained explicitly from

$$\bar{\theta} = \arctan \left\{ \frac{C_{pv}}{C_{pu}} \right\} \qquad , \qquad (31)$$

and

$$\bar{s} = \frac{r_1}{1 - r_1} \qquad , \qquad (32)$$

where

$$r_1^2 = \frac{C_{pu}^2 + C_{pv}^2}{\left[C_{uu} + C_{vv} \right] C_{pp}} \qquad . \qquad (33)$$

The second order estimates are obtained from

$$\bar{\theta} = \frac{1}{2} \arctan \left\{ \frac{2C_{uv}}{C_{uu} - C_{vv}} \right\} \qquad , \qquad (34)$$

and

$$\bar{s} = \frac{(1+3r_2) + (1-14r_2 + r_2^2)^{1/2}}{2(1-r_2)} \qquad , \qquad (35)$$

where

$$r_2^2 = \frac{\left\{ C_{uu} - C_{vv} \right\}^2 + 4C_{uv}^2}{C_{uu} + C_{vv}} \qquad . \qquad (36)$$

It should be noted that these estimates are derived from measurements
of wave kinematics which have suffered frequency dependent depth
attenuation. As the depth of measurements increases, these estimates
become more biased towards longer period waves.

6.   INSTRUMENT PERFORMANCE

Local deployments of the Sea Data 635-12S Directional Wave and Tide
Recorder have now returned in excess of two years of data.
Improvements in the design and operation of the instrument, and in the
data transcription and processing techniques, now allow better than
98% data recovery.

Experience with deployments at various locations around Australia
shows that minimum wave periods of 2, 5 and 8 seconds may be
satisfactorily resolved in water depths of 2, 20 and 50 metres,
respectively. The directionality of recorded wave fields has been
evident in all deployments.

The performance of the 635-12S is illustrated by measurements
conducted in 20 metres of water at a location 30 km south of Barrow
Island off the north west coast of Australia, during the passage of
tropical cyclone "Chloe". The measurement location and tropical
cyclone track are shown in figure 3. The storm track passed about
150 km to the south east of the measurement location.
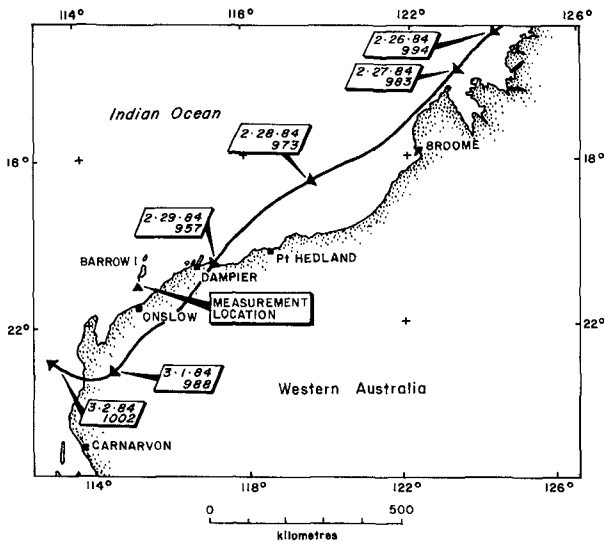

Figure 3   Location diagram showing directional wave measurement site
           and the track of tropical cyclone "Chloe". Arrow heads on
           the track correspond to 1200 hours GMT. Date and storm
           central pressure (mb) are shown adjacent each mark.

Figure 2 shows the directional spectral information obtained from one
"burst" of the 635-12 near the time of closest approach of the storm.
This includes the presentation of θ(f) and s(f) as a function of
frequency, derived from equations (25) to (30). In this figure, the
distinct bimodality of the sea state is evident, with swell waves
(periods longer than 8 seconds) propagating from the north west, and
short period, locally generated wind waves propagating from the south.

Averages weighted by the non-directional energy spectrum were taken to
produce burst mean estimates, denoted by θ̂ and ŝ. Figure 4 shows the
variation of the directional wave climate during the passage of
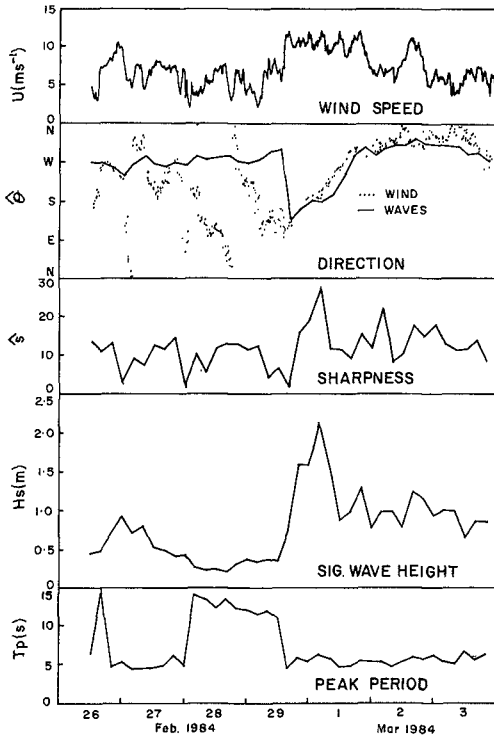tropical cyclone "Chloe", using burst mean parameters.

Figure 4   Description of the temporal variation of the directional
           climate using mean spectral parameters, for the period of
           the passage of tropical cyclone "Chloe".

Wind speeds and directions shown are 20 minute mean values recorded on
Barrow Island, about 30 km north of the measurement location. The
first order estimate of the wave direction $\hat{\theta}$, initially shows the
incidence of westerly to north westerly swell, then tracks the wind
direction after the onset of the storm. The sharpness index $\hat{s}$ peak is
observed to coincide with the storm peak, as also noted by Mitsuyasu
et al. (1975).

Non-directional spectral parameters H_s (significant wave height) and
T_p (period of the spectral peak) illustrate the incidence of low
amplitude, long period swell prior to the arrival of the storm,
followed by the generation of a high energy, short period sea state.

The 635-12S may also be used to establish frequency dependent
variations in the wave climate. This is achieved by taking averages
of E(f), s(f), θ(f) and Q(f) for each spectral ordinate over entire
deployments. Figure 5 illustrates the result of averaging the
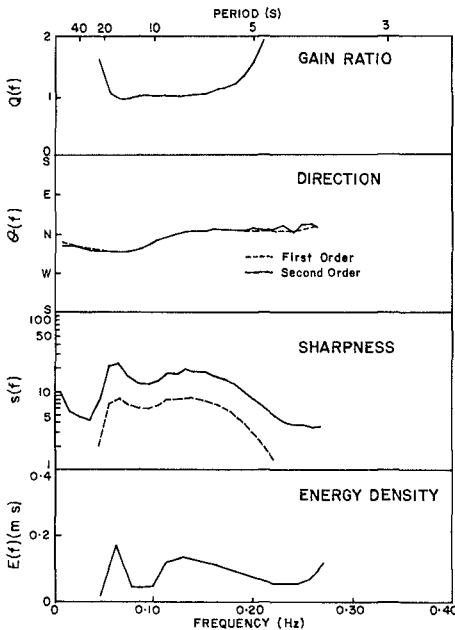spectral parameters over a six week deployment period.

Figure 5   Spectral parameter means providing a description of the
           frequency dependent variation of the directional wave
           climate, over the period of an entire deployment.

Q(f) determines the limits of applicability of the frequency dependent
wave climate description, which holds only while Q(f) is near unity.
Within this frequency range, the wave climate is seen to be distinctly
bimodal, with swell periods in excess of 10 seconds typically incident
from the north west, and shorter period wind waves (6 to 10 seconds)
typically incident from the north-north-east. For this deployment,
bathymetric constraints limit wave propagation from the east. The
sharpness and energy density estimates also reflect the bimodality of
the wave climate.

Comparison of Analysis Techniques :   Figure 2 shows that first and
second order estimates of θ are very similar. Estimates of s vary,
but they do display similar trends.

Estimates of $\bar{\theta}$ and $\bar{s}$ may be obtained without recourse to spectral
analysis, using the covariance equations (31) to (36). A comparison
of these estimates with their spectral equivalents, $\hat{\theta}$ and $\hat{s}$, weighted
by the energy density) is presented in figure 6, again using data
recorded during the passage of tropical cyclone "Chloe".
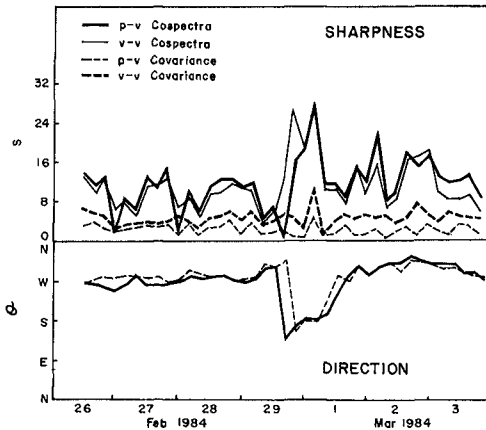

Figure 6   Comparison of mean wave directions and sharpness indices
           derived by time domain (covariance estimates $\bar{\theta}$ and $\bar{s}$) and
           frequency domain (cospectral estimates $\hat{\theta}$ and $\hat{s}$) techniques.

First and second order estimates of θ in either the time domain
(covariances) or frequency domain (cospectra), are almost
indistinguishable. However, small differences are evident between
time domain and frequency domain estimates, particularly during
periods of rapid change in the sea state.

First and second order estimates of s show the expected similar
trends, but time domain estimates are generally less than the
frequency domain estimates.

Comparison with Surface Wave Measurements :   A Datawell Waverider
buoy was deployed concurrently with the Sea Data 635-12S, at the same
location during the passage of tropical cyclone "Chloe". This allowed
comparison of non-directional wave parameter estimates, which are
presented in figure 7.
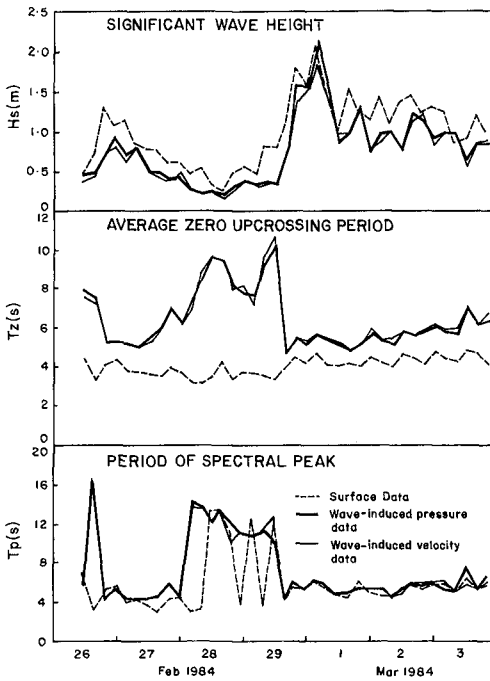

Figure 7   Comparison of non-directional spectral surface wave
           parameters derived from surface displacement measurements,
           and near-bottom pressure and velocity measurements.

Estimates of significant wave height derived from both near-bottom
pressure and velocity measurements agree very well, except at the
storm peak where dynamic pressure effects may have become important.
Generally, Waverider estimates of significant wave height exceed those
derived from the near-bottom measurements due to the depth attenuation
of short period waves (5 seconds or less). At the storm peak,
estimates from the Waverider and the near-bottom pressure measurements
coincide.

Estimates of average zero upcrossing period and spectral peak period
derived from both near-bottom pressure and velocity measurements also
agree very well. While Waverider measurements provide good agreement
for spectral peak period, average zero upcrossing periods are seen to
be much lower than those derived from near-bottom measurements,
because of the predominance of short period surface waves.

In accordance with Forristall et al. (1978), comparisons of measured
near-bottom wave-induced velocity spectra with those derived from
surface wave measurements using non-directional linear wave theory,
show the theory to overpredict near-bottom velocities by about 20%.

7.   COMMENTS AND CONCLUSIONS

The Sea Data 635-12S Directional Wave and Tide Recorder provides a
reliable means of measurement of near-bottom wave-induced kinematics
and of shallow water directional wave climate.

Uni-directional linear wave theory is seen to overpredict near-bottom
wave-induced velocities derived from surface wave measurements.

A variety of analysis techniques are available, several of which have
been applied to the measured data. Analyses undertaken to date have
not indicated a preference for first or second order estimates of
directional wave parameters. Maximum likelihood techniques which
combine both estimates have been successfully applied to simulated
data, but small (sensor induced) phase differences between measured
pressures and velocities inhibit application to field data. It is
hoped to apply these types of data adaptive techniques in the future.

The Sea Data 635-12S Directional Wave and Tide Recorder can routinely
provide important information for determination of wave-induced forces
on coastal structures and submarine pipelines, for shallow water wave
refraction and diffraction studies and for sediment transport studies.

8.   REFERENCES

Aubrey, D.G. and W. Hill, 1984. Performance of bottom-mounted
     directional wave gauges. Conference Record, Oceans '84, Marine
     Technology Society, IEEE Ocean Engineering Society, Washington
     D.C.

Borgman, L.E., 1979. Directional wave spectra from wave sensors. In
     Ocean Wave Climate edited by M.D. Earle and A. Malahoff. Marine
     Science, 8, 269-300. Plenum Press (N.Y.).

Forristall, G.Z., Ward, E.G., Cardone, V.J. and Borgman, L.E., 1978.
    The directional spectra and kinematics of surface gravity waves
    in tropical storm Delia. J. Phys. Oceanogr., 8, 888-909.

Goda, Y., Takayama, T. and Y. Suzuki, 1978. Diffraction diagrams for
    directional random waves. Proc. 16th Coastal Eng. Conf. Hamburg.
    Published by ASCE, New York.

Grosskopf, W.G., Aubrey, D.G., Mattie, M.G. and M. Mathiessen, 1983.
    Field intercomparison of nearshore directional wave sensors.
    IEEE J. Oceanic Eng., OE-8, 254-271.

Longuet-Higgins, M.S., Cartwright, D.E. and N.D. Smith, 1963.
    Observations of the directional spectrum of sea waves using the
    motions of a floating buoy. Ocean Wave Spectra, Prentice-Hall
    Inc. (NY), pp. 111-136.

Mitsuyasu, J., Tasai, F., Suhara, T., Mizuno, S., Ohkusu, M., Honda,
    T. and K. Rikiishi, 1975. Observations of the directional
    spectrum of ocean waves using a cloverleaf buoy. J. Phys.
    Oceanogr., 5, 750-760.

Sand, S.E., Brink-Kjaer, O. and J.B. Nielson, 1981. Directional
    numerical models as a design basis. ARAE International
    Symposium, Wave and Wind Directionality with Applications to the
    Design of Structures. Paris.